Free Radical Biology and Medicine 86 (2015) 239–249

Contents lists available at ScienceDirect

Free Radical Biology and Medicine

journal homepage: www.elsevier.com/locate/freeradbiomed

Original Contribution

A subset of N-substituted phenothiazines inhibits NADPH oxidases

Tamara Seredenina [a], Gianpaolo Chiriano [b], Aleksandra Filippova [a], Zeynab Nayernia [a], Zahia Mahiout [a], Laetitia Fioraso-Cartier [a], Olivier Plastre [a], Leonardo Scapozza [b], Karl-Heinz Krause [a,c,1], Vincent Jaquet [a,*,1]

[a] Department of Pathology and Immunology, Medical School, School of Pharmaceutical Sciences, University of Geneva, 1211 Geneva 4, Switzerland
[b] Pharmaceutical Biochemistry Group, School of Pharmaceutical Sciences, University of Geneva, 1211 Geneva 4, Switzerland
[c] Department of Genetic and Laboratory Medicine, Geneva University Hospitals, Geneva, Switzerland

ARTICLE INFO

Article history:
Received 22 January 2015
Received in revised form
15 May 2015
Accepted 15 May 2015
Available online 23 May 2015

Keywords:
NADPH oxidase
ROS
NOX inhibitor
SAR
Phenothiazine
Thioridazine
Fibrosis
Free radicals

ABSTRACT

NADPH oxidases (NOXs) constitute a family of enzymes generating reactive oxygen species (ROS) and are increasingly recognized as interesting drug targets. Here we investigated the effects of 10 phenothiazine compounds on NOX activity using an extensive panel of assays to measure production of ROS (Amplex red, WST-1, MCLA) and oxygen consumption. Striking differences between highly similar phenothiazines were observed. Two phenothiazines without N-substitution, including ML171, did not inhibit NOX enzymes, but showed assay interference. Introduction of an aliphatic amine chain on the N atom of the phenothiazine B ring (promazine) conferred inhibitory activity toward NOX2, NOX4, and NOX5 but not NOX1 and NOX3. Addition of an electron-attracting substituent in position 2 of the C ring extended the inhibitory activity to NOX1 and NOX3, with thioridazine being the most potent inhibitor. In contrast, the presence of a methylsulfoxide group at the same position (mesoridazine) entirely abolished NOX-inhibitory activity. A cell-free NOX2 assay suggested that inhibition by N-substituted phenothiazines was not due to competition with NADPH. A functional implication of NOX-inhibitory activity of thioridazine was demonstrated by its ability to block redox-dependent myofibroblast differentiation. Our results demonstrate that NOX-inhibitory activity is not a common feature of all antipsychotic phenothiazines and that substitution on the B-ring nitrogen is crucial for the activity, whereas that on the second position of the C ring modulates it. Our findings contribute to a better understanding of NOX pharmacology and might pave the path to discovery of more potent and selective NOX inhibitors.

Introduction

NADPH oxidases (NOXs) are important cellular sources of reactive oxygen species (ROS) involved in diverse key physiological functions, such as microbial killing, hormone synthesis, and production of the otoliths of the inner ear. NOX enzymes are a family of transmembrane proteins comprising seven members (NOX1–NOX5 and DUOX1 and DUOX2), each with a specific tissue distribution and activation mechanism [1]. They catalyze the reduction of molecular oxygen to superoxide anion, which in turn reacts quickly to generate other ROS, such as hydrogen peroxide [2]. Although basic NOX activity is crucial for normal physiology, overshooting activity of NOX enzymes leads to disease. Indeed, accumulating evidence from animal studies shows that genetic deletion of NOX enzymes, mostly NOX1, NOX2, and NOX4, is protective in animal models against neurodegeneration [3], fibrotic diseases [4], and cardiovascular diseases [5], among others [6–8]. These findings using genetically modified mice provide a strong rationale for identifying small-molecule NOX inhibitors for pharmacological targeting of NOX enzymes. Despite increasing efforts of academia and pharmaceutical laboratories, the development of specific NOX inhibitors is still at its beginning, and nonspecific inhibitors are often used to study the involvement of NOX enzymes in biological processes (for a recent comprehensive review of documented small-molecule NOX inhibitors, see [9].

A major challenge for the development of NOX inhibitors is the fact that detection of NOX activity through ROS measurements is a

Abbreviations: CHO, Chinese hamster ovary; DMSO, dimethyl sulfoxide; DUOX, dual oxidase; DMEM, Dulbecco's modified Eagle medium; DPI, diphenyleneiodonium; ESP, electrostatic potential; FBS, fetal bovine serum; GFP, green fluorescent protein; HBSS, Hanks' buffered salt solution; HEK, human embryonic kidney; MCLA, 2-methyl-6-(4-methoxyphenyl)-3,7-dihydroimidazo[l,2-*a*]pyrazin-3(7*H*)-one hydrochloride; NOX, NADPH oxidase; NOXO1, NADPH oxidase organizer type 1; PBS, phosphate-buffered saline; PKC, protein kinase C; PMA, phorbol myristate acetate; RPMI, Roswell Park Memorial Institute; ROS, reactive oxygen species; SAR, structure–activity relationship; WST-1, 2-(4-iodophenyl)-3-(4-nitrophenyl)-5-(2, 4-disulfophenyl)-2*H*-tetrazolium, monosodium salt

* Corresponding author. Fax: +41 22 379 41 32.
E-mail address: Vincent.Jaquet@unige.ch (V. Jaquet).
[1] These authors equally contributed to this study.

http://dx.doi.org/10.1016/j.freeradbiomed.2015.05.023
0891-5849/

complex task prone to artifacts [10,11]. Compounds thought to directly inhibit NOX enzymes were later identified as having different modes of action, including antioxidant [12], peroxidase inhibition, and assay interference [13,14]. Therefore a robust reliable screening cascade should be implemented to identify and characterize novel NOX inhibitors.

Phenothiazines are three-cyclic compounds. The parent compound is phenothiazine itself, which was used as an antihelminthic and later served as a backbone for designing multiple antipsychotics through substitutions at ring B and ring C (Fig. 1). The antipsychotic activity of phenothiazine derivatives is mostly due to inhibition of dopamine D2 receptors [15]. However, phenothiazine compounds also have additional targets [16]. In particular, they have been shown to inhibit cellular ROS generation [17] possibly through direct inhibition of NOX enzymes [18,19].

In this study, we investigated the NOX inhibitory effect of 10 commercially available molecules of the phenothiazine family. We present an extensive panel of assays including ROS measurements using chemically diverse probes, measurement of oxygen consumption by NOX enzymes, cell-free assays, and orthogonal assays to identify off-target effects. Using this approach, we were able to identify striking differences in the NOX-inhibitory activity inside the group of chemically similar phenothiazines and show that N-substituted phenothiazines such as thioridazine, prochlorperazine, and perphenazine are bona fide NOX inhibitors, whereas unsubstituted phenothiazines such as the parent compound phenothiazine and 2-acetylphenothiazine (aka ML171 [19]) are not NOX inhibitors, but interfere with peroxidase-dependent ROS-measuring assays. Finally, we established the biological relevance of NOX inhibition in an in vitro functional assay by showing that

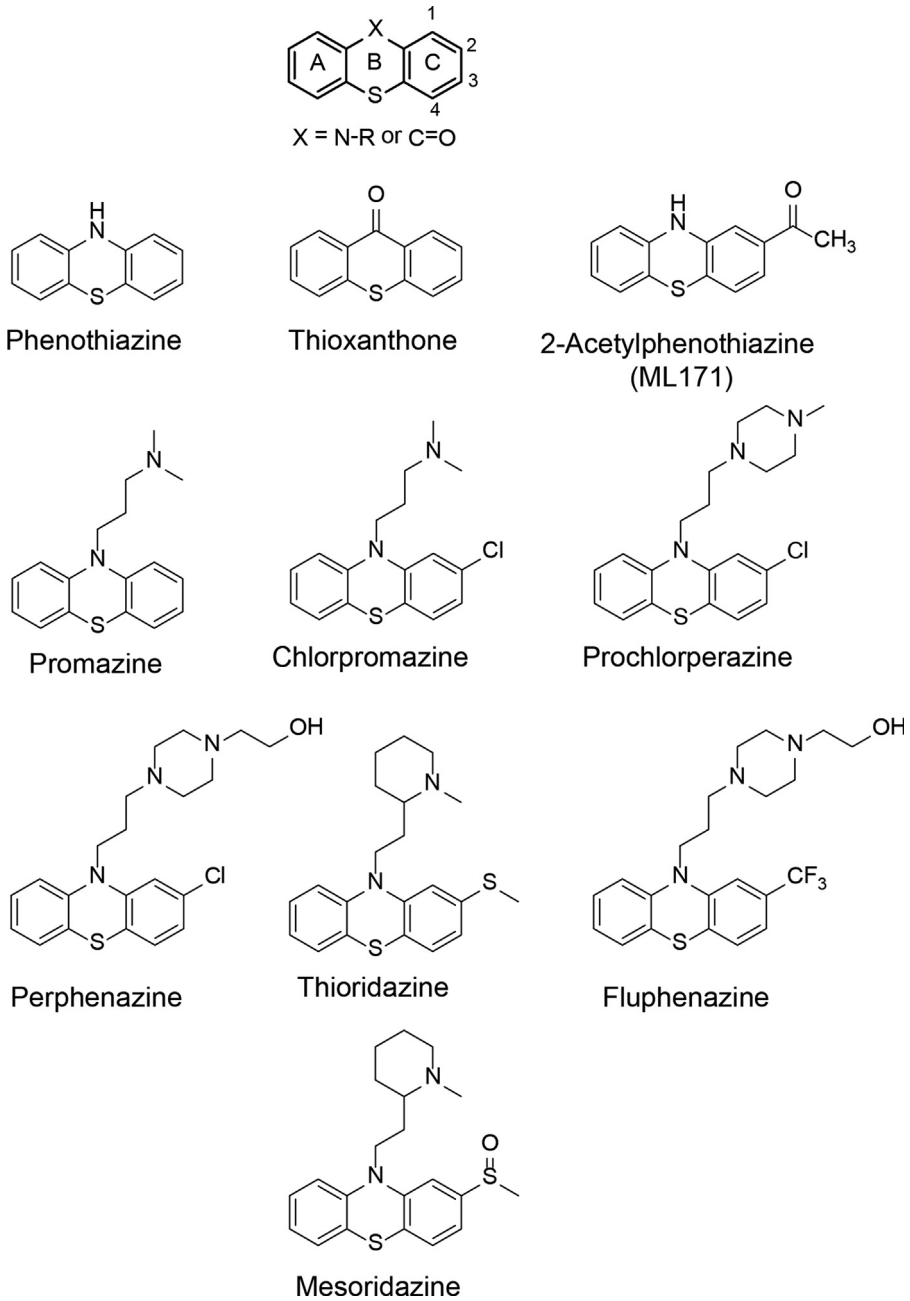

Fig. 1. Chemical structures of compounds of the phenothiazine family used in the study. Anthracene is the skeleton of the phenothiazine family and is composed of three rings (A, B, C); the numbering used is indicated. Phenothiazine is the compound in which X=NH, thioxanthone is the compound in which X=CO, and promazine is the simpler N-substituted derivative. All other molecules have additional substitutions on position 2 in the C ring.

thioridazine—but not phenothiazine—inhibits redox-dependent differentiation of human fibroblasts into myofibroblasts.

Methods

Chemicals and reagents

Dulbecco's modified Eagle medium with 4.5 g/L glucose (DMEM), Roswell Park Memorial Institute (RPMI) 1640 with Glutamax, Hanks' buffered salt solution (HBSS), fetal bovine serum (FBS), 2-methyl-6-(4-methoxyphenyl)-3,7-dihydroimidazol[1,2–a] pyrazin-3-one hydrochloride (MCLA), and Amplex red were purchased from Invitrogen. Phenothiazine, thioxanthone, thioridazine hydrochloride, prochlorperazine dimaleate salt, promazine hydrochloride, perphenazine, fluphenazine hydrochloride, mesoridazine benzene sulfonate, chlorpromazine hydrochloride, 2-acetylphenothiazine, penicillin, streptomycin, phorbol myristate acetate (PMA), calcein, diphenyleneiodonium chloride (DPI), dextran sulfate, dimethyl sulfoxide (DMSO), Tween 20, and carboxymethylcellulose sodium were purchased from Sigma–Aldrich. Ficoll-Paque Plus was purchased from Amersham Biosciences (Uppsala, Sweden). 2-(4-Iodophenyl)-3-(4-nitrophenyl)-5-(2,4-disulfophenyl)-2*H*-tetrazolium, monosodium salt (WST-1) was from Dojindo Molecular Technologies.

Cells

Details of NOX-expressing cell lines are summarized in Table 1. Human neutrophils were isolated from fresh whole blood collected from healthy volunteers as described [37]. Cell lines with heterologous expression of NOX1 [37], NOX4, and NOX5 isoforms were described previously [18,38]. The NOX2-expressing cells were PLB-985 myeloid cells and PLB-985 differentiated into granulocyte-like cells by the addition of DMSO (1.25%) to the medium for 72 h [39]. The HEK-NOX3 cell line was generated in the following way: the coding sequences of NOX3, NOXO1, NOXA1, and $p22^{phox}$ were amplified using Phusion high-fidelity DNA polymerase (New England Biolabs) with Gateway (Invitrogen) adaptable primers. NOX3 was amplified from a human embryonic kidney cDNA library (Clontech, No. 636584), NOXO1 and NOXA1 were amplified as previously described [40], and $p22^{phox}$ was amplified from cDNA generated using human neutrophil RNA. The sequences were inserted first into pDONR 221 (Invitrogen) and then subcloned into the 2K7 vector [41] with the cytomegalovirus (CMV) promoter and a tetracycline-inducible CMV promoter for NOX3. The vectors for NOX3, NOXO1, NOXA1, and $p22^{phox}$ contained GFP, zeocin, neomycin, and blasticidin, respectively, as a means of selection. All cells were cultured in DMEM/F12 (1/1), or RPMI 1640 for PLB-985 cells, supplemented with FBS (10%), penicillin (100 U/ml), and streptomycin (100 μg/ml) at 37 °C in air with 5% CO_2.

ROS measurements in intact cells

Cells were collected by trypsinization for adherent cells (CHO, HEK) or centrifugation for cells in suspension (PLB-985), washed with HBSS, counted, and resuspended in HBSS at 500,000 cells/ml. Cells were seeded in 96-well plates at a density of 50,000 cells (100 μl). Black flat-bottom plates were used for fluorescence and chemiluminescence and transparent plates for absorbance readouts. All compounds were dissolved in DMSO and concentrations ranging from 50 to 0.35 μM were tested in NOX cellular assays with a final concentration of DMSO of 0.5%. Cells were incubated with the compounds for 10 min before measurement. Cells expressing NOX1 and NOX2 were activated with the PKC activator PMA (0.1 μM), and NOX5 was activated with the Ca^{2+} ionophore ionomycin (1 μM). Tetracycline (1 μg/ml) was added to the medium of tetracycline-inducible HEK-NOX4 and HEK-NOX3 cells for 18 h before measurement. Production of hydrogen peroxide by NOX in intact cells was measured using Amplex red fluorescence as described [37]. Production of the superoxide anion was measured by the maximal chemiluminescence of 20 μM MCLA [42] and the absorbance change rate of 100 μM WST-1 at 440 nm. WST-1 is a formazan salt specifically reduced by the superoxide anion. The usefulness of WST-1 for detection of NOX activity was elegantly validated by Tan and Berridge [22]. The specificity of WST-1 for NOX2 activity was validated by using specific NOX2 activation by PMA (100 nM) and a short measurement time (30 min). Fluorescence, chemiluminescence, and absorbance were measured in a FluoSTAR Optima, BMG Labtech instrument at 37 °C.

ROS measurement in NOX2 membrane assay

To prepare NOX2-containing membranes, differentiated PLB-985 cells (approximately 10^7 cells) were homogenized in 1.5 ml of a sonication buffer containing PBS (0.1 ×), sucrose (11%), NaCl (120 mM), and EGTA (1 mM) supplemented with protease inhibitors (Complete Mini, Roche) and processed as described [37]. Measurement of ROS generation by NOX2-containing membranes was performed by MCLA luminescence (area under the curve) as previously described [43,44]. Briefly, 1 μl of various concentrations of compounds dissolved in DMSO was incubated in 80 μl of a mix containing NOX2 membranes (0.5 μg of protein), 0.25 μg p67Np47N chimeric protein (a fusion of the N termini of human $p67^{phox}$ (residues 1–210) and $p47^{phox}$ (residues 1–286)), 0.2 μg Rac1Q61L, 0.025 μM FAD, 90 μM SDS, and 30 μM MCLA in 1 × Dulbecco's PBS (Gibco, Life Technologies). After 5 min at room temperature, the reaction was initiated by addition of 20 μl NADPH (final 20 μM). Luminescence was immediately measured in a FluoSTAR Optima, BMG Labtech luminometer at 37 °C. For competition assays, serial dilutions of NADPH (0–200 μM) were added. Plasmids expressing recombinant proteins were kindly

Table 1
NOX-expressing cell lines used in this study.

NOX enzyme	Cell line/expression type	Expressed subunits	Activation reagent	Ref.
NOX1	CHO/heterologous expression	NOX1, CYBA, NOXO1, NOXA1	PMA 0.1 μM	[37]
NOX2 (CYBB)	PLB-985/natural expression after differentiation with 1.25% DMSO for 72 h	—	PMA 0.1 μM	[39]
NOX3	T-REx 293/heterologous expression	NOX3, CYBA, NOXO1, NOXA1	Tetracycline 1 μg/ml, 24 h before experiment	This study
NOX4	T-REx 293/heterologous expression	NOX4	Tetracycline 1 μg/ml, 24 h before experiment	[18]
NOX5	HEK-293/heterologous expression	NOX5	Ionomycin 1 μM	[38]

provided by Dr. Becky Diebold, Emory University (Atlanta, GA, USA).

Oxygen consumption

Human polymorphonuclear cells were isolated from fresh whole blood collected from healthy volunteers as described previously [45], using Ficoll-Paque Plus (Amersham Biosciences), and resuspended in HBSS buffer. Oxygen consumption was measured using a Clarke electrode as described before [37] or using a Seahorse XFe24 machine. Neutrophils were plated in 24-well microplates (250,000 cells/well in 200 μl HBSS) and incubated at room temperature for 15 min to let them attach. The medium was then changed for DMEM without sodium bicarbonate containing 10 mM Hepes, and the cells were incubated for 30 min at 37 °C in a non-CO_2 incubator. Basal levels of oxygen consumption were recorded for 8 min followed by 8 min preincubation with compounds. PMA (100 nM) was added where indicated and the oxygen consumption rate was determined for two cycles of 8 min each. The second measurement upon PMA addition was used to evaluate the effects of compounds on oxygen consumption. Signal from neutrophils without PMA treatment was taken as 0 and signal from PMA+DMSO-treated neutrophils was considered as 100%. At least three independent experiments were performed for each compound.

Real-time quantitative polymerase chain reaction

RNA was extracted from human fibroblasts using the Qiagen RNeasy mini kit. Five hundred nanograms was used for cDNA synthesis using the Takara PrimeScript RT reagent kit and following the manufacturer's instructions. Real-time PCR was performed using the SYBR green assay at the Genomics Platform, National Center of Competence in Research Frontiers in Genetics (Geneva, Switzerland), on a 7900HT SDS system from ABI. The efficiency of each primer was assessed with serial dilutions of cDNA. Relative expression levels were calculated by normalization to the geometric mean of two housekeeping genes, β2-microglobulin and GAPDH, as described previously [46]. The highest normalized relative quantity was arbitrarily designated a value of 1.0. Fold changes were calculated from the quotient of the means of these normalized quantities and reported as ± SEM. The sequences of the primers used in this study are shown in Supplementary Table 1. The C_t value range for control treatments is presented in Supplementary Table 2.

Human foreskin fibroblast differentiation

The human foreskin fibroblast cell line CCD-1112Sk (ATCC CRL-2429) was maintained in DMEM supplemented with FBS (10%), penicillin (100 U/ml), and streptomycin (100 μg/ml) at 37 °C in air with 5% CO_2. For differentiation experiments, the cells were kept in a serum-free medium for 24 h and treated with 2 ng TGF-β1 with either DMSO or the compounds for another 24 h and collected for protein or RNA extraction or immunofluorescence.

Immunofluorescence

Cells were washed in PBS, fixed in 4% paraformaldehyde for 15 min, rinsed three times in PBS, permeabilized with 0.5% Triton X-100 for 5 min, blocked with 5% bovine serum albumin, and incubated with primary antibody against α-smooth muscle actin (α-SMA; Sigma A2547, 1:250) for 2 h at room temperature followed by secondary antibody, anti-mouse Alexa Fluor 555 (Molecular Probes A21424, 1:1000), for 1 h at room temperature. Incubation with DAPI was performed to visualize nuclei. Coverslips were mounted using FluorSave reagent (Millipore). Images were taken with a Leica SP5 confocal microscope (DM6000) using Leica LAS system software.

Cell viability

The effects of the compounds on cell viability was evaluated using a calcein-AM (Invitrogen) assay. HEK-293T-REx, PLB-985, or CHO cells (0.5×10^6/ml) were pre-incubated with compounds for 10 min at room temperature in HBSS, then the reaction mixture containing 2 μM calcein was added and incubated for 30 min at 37 °C. Single-point fluorescence measurements were then made with a microplate reader (FluoSTAR Optima, BMG Labtech) at 485 nm excitation/520 nm emission for calcein.

Ligand preparation and electrostatic potential (ESP) surface calculations

All the compounds were modeled by using the Maestro program (Schrödinger LLC, Portland, OR, USA; 2009), a tool from the Schrödinger 2013 package. Energy minimizations were carried out in water by applying 10,000 iterations with a conjugated gradient of 0.05 kcal/mol and using the OPLS-2005 force field. Geometric optimizations of compounds were carried out in implicit water solvent. The ESP surfaces were calculated by using the Poisson–Boltzmann method at the temperature of 298 K (solute dielectric constant, 1.0; solvent dielectric constant, 80; solvent radius, 1.4 Å). ESP surfaces were plotted between −4.0 and +4.0 a.u.

Statistical analysis

Data were analyzed using GraphPad Prism software 5.0. For the inhibition dose–response curves of ROS generation as detected by Amplex red, MCLA, and WST-1, sigmoidal dose–response curves were fitted, from which half-maximal efficient concentration (EC_{50}) values were obtained ($n=3$ or 4). Toxicity data are presented as a percentage of control ($n=3$), the data of the whole-blood assay are presented as a percentage of inhibition compared to absence of inhibitor (PMA alone) ($n=3$ or 4), and the rate of oxygen consumption (nmol/min/10^7 cells) was calculated for oximeter data ($n=3$).

Results and discussion

Evaluation of the effects of phenothiazine compounds on NOX-derived ROS generation

To identify small-molecule NOX inhibitors, we performed a screen of a National Institute of Neurological Disorders and Stroke library using PMA-activated neutrophils and luminol-enhanced luminescence as a readout (data not shown). Among the identified hits, the neuroleptic drug thioridazine strongly inhibited luminol chemiluminescence and was further analyzed. A literature search indicated that compounds of the phenothiazine family can decrease ROS generation by NOX2 in granulocytes and macrophages [17,20] and even NOX4 activity [18], but formal evidence of NOX inhibition was not proven, as this effect was mostly attributed to ROS-scavenging activity [21]. We therefore tested the effect of phenothiazine molecules structurally related to thioridazine (Fig. 1) on ROS production in a panel of cellular assays using two structurally unrelated probes, Amplex red and MCLA. Cell lines expressing the various isoforms of NOX1–5 were incubated in the presence of increasing concentrations of each compound. ROS generation was induced by PMA for NOX1 and NOX2, preincubation with tetracycline for NOX3 and NOX4, and

ionomycin stimulation for NOX5. Extracellular hydrogen peroxide could be measured for all cell lines using the Amplex red assay, but superoxide anion generation was detected by MCLA chemiluminescence only for NOX1, NOX2, and NOX5. The effects of compounds on the activity of DUOX enzymes was not evaluated in this study. Representative concentration-dependent inhibition curves are shown for thioridazine, mesoridazine, and phenothiazine (Fig. 2). Thioridazine was active in both assays (Figs. 2a and 2g); mesoridazine was inactive in both assays (Figs. 2b and 2h), and phenothiazine was active only in the Amplex red assay (Figs. 2c and 2i). An orthogonal assay using Amplex red components in the presence of 10^{-5} M hydrogen peroxide (without cells) detected an off-target effect of phenothiazine on the assay (Fig. 2f). Thioridazine and mesoridazine were inactive in the Amplex red orthogonal assay (Figs. 2d and 2e). The specificity of thioridazine over phenothiazine was further confirmed using the colorimetric probe WST-1 [22] as a second mechanistically distinct superoxide-dependent assay (Figs. 2j, 2k, and 2l). A potential cytotoxic effect of the compounds was tested in the calcein cell viability assay (Figs. 2m, n, and o and Supplementary Fig. 3S). Cytotoxicity was observed only for higher concentrations of thioridazine (≥ 25 μM; Fig. 2m), indicating that the observed inhibition was not due to cellular toxicity. Potential fluorescence quenching of unsubstituted phenothiazines was excluded as the fluorescent signal was not decreased when the compounds were added after the reaction was completed (data not shown). A total of 10 phenothiazine-related compounds were tested using a similar approach. A summary of the calculated IC_{50} values for each NOX isoform and each probe is documented in Table 2. We found that despite high structural similarities, the effects on NOX inhibition were significantly different.

Structure–activity relationships of phenothiazines

To address these differences we performed structure–activity relationship (SAR) analysis of the phenothiazine derivatives based on their IC_{50} values against NOX2 determined in the cell-based Amplex red assay (see Table 2 and Fig. 3). As reported in Table 2, the two undecorated scaffolds tested, phenothiazine and thioxanthone, do not display any inhibition against NOX2. The apparent inhibition observed for the phenothiazine moiety in the Amplex red assay ($IC_{50} = 1.6 \pm 0.3$) is due to its interference with the assay (H_2O_2 $IC_{50} = 1.0 \pm 0.4$), potentially due to either the intrinsic antioxidant power of the molecule or the inhibition of horseradish peroxidase. This consideration can also be done for 2-acetylphenothiazine (aka ML171), which was previously described as a specific NOX1 inhibitor in a screen using the peroxidase-dependent probe luminol [19]. Our results indicate that 2-acetylphenothiazine is inactive on all NOX isoforms, including NOX1, but interferes with the Amplex red assay. This finding is in line with two recent studies by Zielonka et al., which critically address the common use of peroxidase-dependent assays, as it increases the probability of identification of false positives, which are in fact inhibitors of the peroxidase mechanism [13,14]. In the case of promazine, the introduction of the aliphatic dimethylpropylamine chain on the N atom of the phenothiazine moiety has a double impact. This causes a loss of its antioxidant/peroxidase action but, on the other hand, remarkably contributes to its inhibitory profile against the NOX enzymes. Promazine is the only phenothiazine tested that shows isoform specificity for NOX2 and NOX4 over other isoforms. All other tested phenothiazine derivatives except for mesoridazine bearing an electron-attracting substituent at position 2 and different aliphatic amine chains (propyl, piperidine, or piperazine) on the N atom of the phenothiazine moiety showed inhibition of NOX1–5.

Correlation between electronic properties of phenothiazines and NOX2 inhibition

Based on the principle that an interaction occurs only if the electrostatic potentials of the surfaces of two interacting moieties are complementary [23] we inspected the possible correlations between the electronic properties of compounds and NOX2 inhibition by calculating the ESP surfaces for all compounds (Supplementary Fig. 2). This approach highlighted a qualitative relationship between the inhibitory potency on NOX2 and the decreased negative character of the aromatic ring C (Fig. 3). In particular, the less negative the aromatic ring C is, the stronger the NOX2 inhibition is. The presence of an electron-attracting substituent (Cl^- atom for chlorpromazine, prochlorperazine, and perphenazine; CH_3S^- group for thioridazine; CF_3 for fluphenazine) decreases the negative character of the aromatic ring C. This may make this moiety more favorable for establishing the highly directional π–π stacking interactions [24–26] with electron-rich aromatic rings of NOX2 residues and its cofactor NADPH with its electrostatic potential changing during the catalytic cycle from NADPH to NADP and back. Because the type of substituent determines directly the positioning of aromatic rings, face to face or edge to face, in such a π–π stacking by influencing the electrostatic energy, the dispersion interaction, and the exchange repulsion [27], it is reasonable to assume that it is highly discriminating for the binding of a compound within a protein cavity that possesses intrinsic steric constraints owing to its particular shape. Despite the favorable N-substitution on its B ring mesoridazine shows no NOX2 inhibition up to a 50 μM concentration. This is probably due to the presence of the methylsulfoxide group at position 2, which is slightly bulkier and has different electron-attracting characteristics compared to the methylsulfanyl of thioridazine. These subtle modifications are sufficient for rendering the interaction of mesoridazine with the NOX2 enzyme unfavorable because of the highly directional character of the π–π stacking interactions formation, needing a very precise alignment of charges [28]. This computational analysis allowed us to better explain the NOX-inhibition activity trend of the molecules examined in this study. Indeed, we determined a significant correlation between the electrostatic properties of these compounds and their NOX2 IC_{50} values, suggesting that modifications on position 2 of ring C can be a promising medicinal chemistry strategy that can be used to perturb the electronic properties and eventually improve the NOX2 inhibition profile.

Evaluation of the effects of phenothiazine compounds on NOX2-dependent oxygen consumption

The NOX enzymes use oxygen as a substrate to generate the superoxide anion. Therefore, NOX activity can be evaluated by measuring oxygen consumption. We used the XF24 extracellular flux analyzer (Seahorse Bioscience) and/or a Clarke electrode to measure oxygen content in a mixture containing PMA-activated human neutrophils in the presence of various phenothiazine compounds. Phenothiazine (Fig. 4, Supplementary Fig. 3), mesoridazine (Fig. 4), and 2-acetylphenothiazine (Fig. 4) had no effect on the respiratory burst, whereas other N-substituted phenothiazines (thioridazine, perphenazine, and prochlorperazine) showed significant reduction of oxygen consumption at 20 μM (Fig. 4, Supplementary Fig. 3). This observation confirmed that thioridazine, perphenazine, and prochlorperazine do inhibit NOX, whereas phenothiazine, 2-acetylphenothiazine, and mesoridazine are inactive.

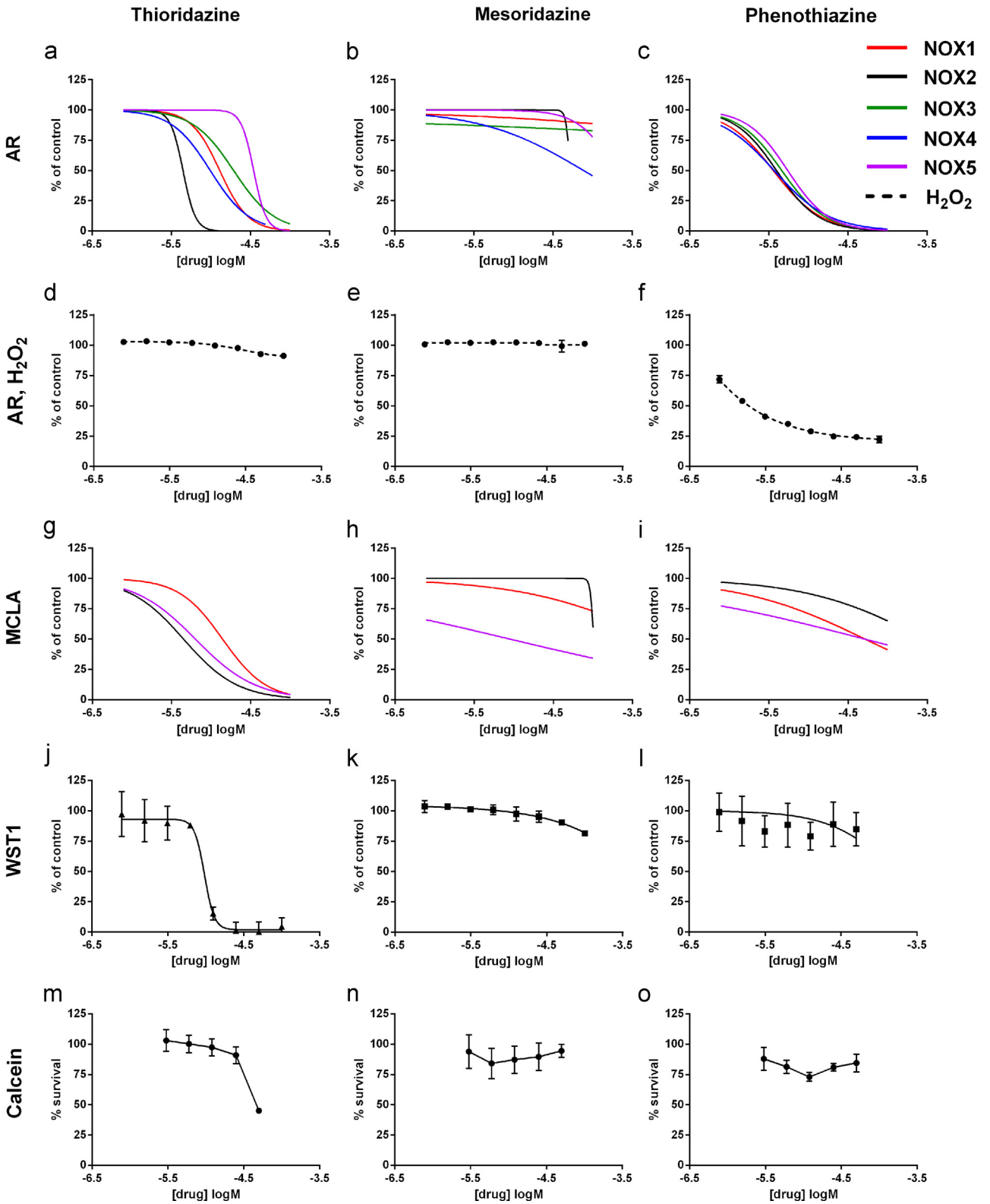

Fig. 2. Concentration–response curves characteristic of NOX inhibition in whole cells. Fluorescence (Amplex red (AR)), chemiluminescence (MCLA), and colorimetric (WST-1) readouts were used to evaluate ROS production by cells treated with phenothiazine derivatives (thioridazine, mesoridazine, phenothiazine). Data were normalized to control responses in each case and fitted using a sigmoidal dose–response curve (GraphPad). AR assay was used for all NOX isoforms and hydrogen peroxide alone and representative curves are shown for (a, d) thioridazine, (b, e) mesoridazine, and (c, f) phenothiazine. MCLA was used for NOX1-, NOX2-, and NOX5-expressing cell lines and inhibitory curves are shown for (g) thioridazine, (h) mesoridazine, and (i) phenothiazine. WST-1 assay was used for NOX2-expressing cells for (j) thioridazine, (k) mesoridazine, and (l) phenothiazine. Values are presented as the mean $\pm$ SD; at least three experiments were performed for each compound. The cytotoxicity of (m) thioridazine, (n) mesoridazine, and (o) phenothiazine was evaluated in HEK cells using calcein-AM fluorescence. Cytotoxicity occurs only at >25 μM for thioridazine.

Table 2
Summary of IC_{50} (μM) of all molecules tested in Amplex red (AR) and MCLA assays.

Name	NOX1		NOX2		NOX3		NOX4		NOX5		H_2O_2
	AR	MCLA	AR	MCLA	AR	MCLA	AR	MCLA	AR	MCLA	AR
Thioridazine	8.0 ± 1.3	6.9 ± 3.3	2.2 ± 0.2	4.3 ± 2.7	11.4 ± 2.0	NA	3.6 ± 1.4	NA	18.8 ± 2.0	2.6 ± 1.4	> 50
Prochlorperazine	10.4 ± 0.8	6.4 ± 1.7	2.4 ± 0.4	4.5 ± 2.4	12.6 ± 4.9	NA	6.0 ± 0.2	NA	13.4 ± 4.2	2.3 ± 1.7	> 50
Perphenazine	10.1 ± 0.8	14.3 ± 7.1	3.9 ± 0.7	12.8 ± 6.1	12.0 ± 1.2	NA	5.0 ± 1.1	NA	11.4 ± 0.8	13.4 ± 5.0	> 50
Chlorpromazine	18.3 ± 2.5	15.9 ± 6.9	4.3 ± 0.9	6.3 ± 3.6	26.9 ± 6.4	NA	> 50	NA	> 50	3.9 ± 3.0	> 50
Fluphenazine	13.1 ± 1.9	11.6 ± 1.5	6.4 ± 1.3	9.1 ± 3.8	14.5 ± 1.4	NA	7.2 ± 1.3	NA	> 50	10.2 ± 3.9	> 50
Promazine	> 50	> 50	7.8 ± 2.2	7.6 ± 1.4	> 50	NA	15.3 ± 4.6	NA	> 50	9.2 ± 5.3	> 50
Phenothiazine **(inactive, interferes with assay)**	1.8 ± 0.1	> 50	1.6 ± 0.3[a]	> 50	1.7 ± 0.6	NA	1.5 ± 0.3	NA	2.8 ± 0.6	> 50	1.0 ± 0.4
2-Acetylphenothiazine **(inactive, interferes with assay)**	1.5 ± 0.9	> 50	1.8 ± 0.9[a]	> 50	0.9 ± 0.4	> 50	4.3 ± 3.6	NA	1.5 ± 0.3	> 50	1.5 ± 1.5
Mesoridazine **(inactive)**	> 50	> 50	> 50	> 50	> 50	NA	> 50	NA	> 50	> 50	> 50
Thioxanthone **(inactive)**	> 50	> 50	> 50	> 50	> 50	NA	> 50	NA	> 50	> 50	> 50

The effects of the compounds were also evaluated on hydrogen peroxide alone (10 μM) using AR. NA, no signal was detected in this assay.
Query to the Author

[a] IC_{50} values represent assay interference and not NOX inhibition.

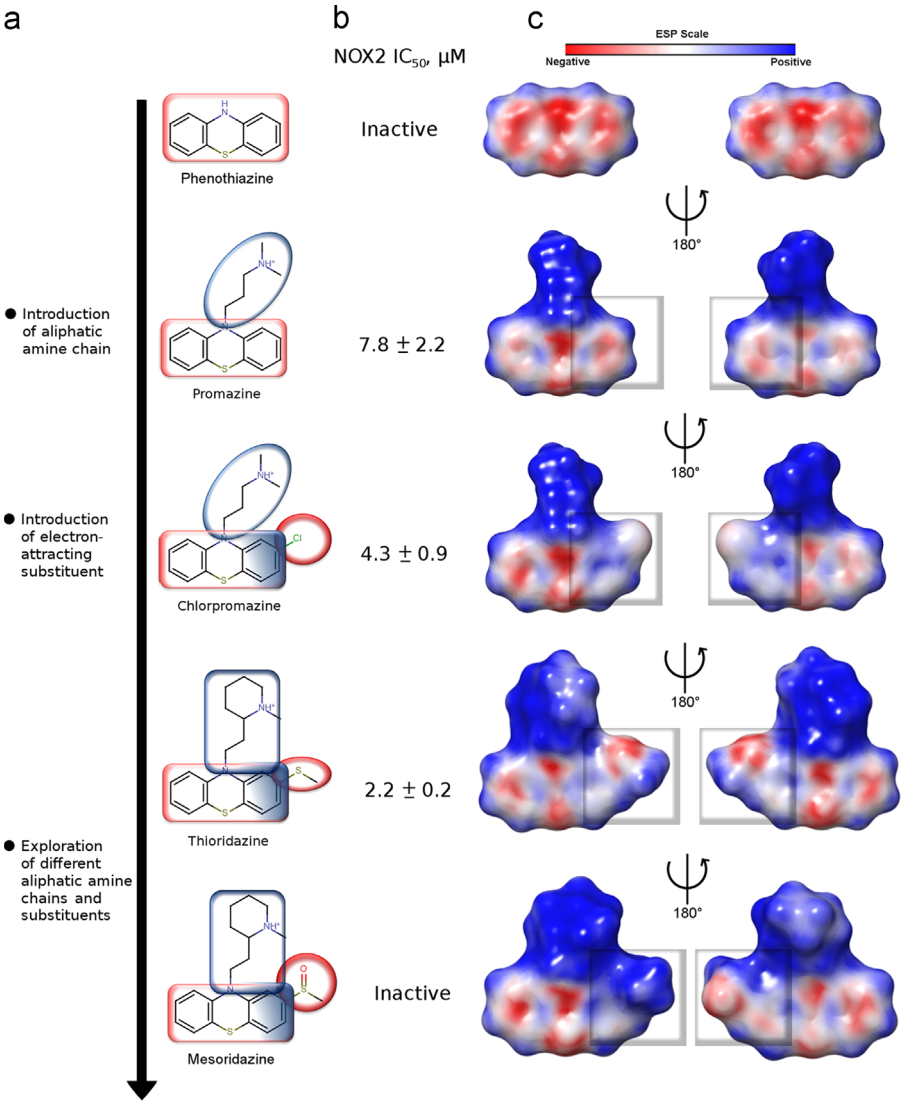

Fig. 3. Structure–activity relationships (SARs) for the phenothiazine derivatives as NOX2 inhibitors. (A) Chemical modifications to explore SARs of phenothiazine derivatives on NOX enzymes. (B) IC_{50} (μM) for NOX2 inhibition obtained in Amplex red assay. Only the values for the molecules that do not interfere with the assay based on H_2O_2 data are shown. (C) Electrostatic potential (ESP) surfaces of phenothiazines substituted differently at N on ring B and at position 2 on ring C of the phenothiazine moiety. According to the NOX2 inhibition data, a concurrent decrease in negative charge (i.e., electron density) of the attached aromatic system can be seen, represented in the ESP surface as a gradual color change from red to white to blue over the phenyl ring. On the top, the ESP scale is presented.

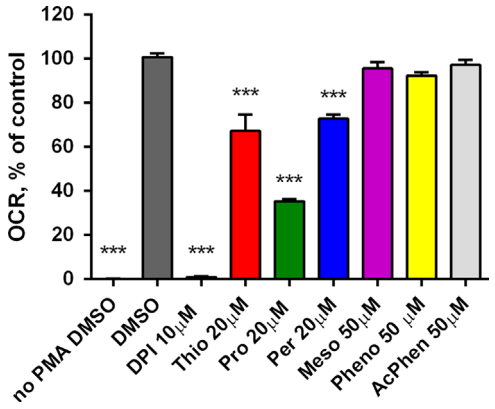

Fig. 4. Effects of selected phenothiazine compounds on oxygen consumption by human granulocytes. Twenty micromolar thioridazine (Thio), prochlorperazine (Pro), and perphenazine (Per) mitigate oxygen consumption in human neutrophils stimulated with 100 nM PMA. Mesoridazine (Meso), phenothiazine (Pheno), and 2-acetylphenothiazine (AcPhen) are inactive at 50 μM. Values are presented as the mean ± SEM. Student's *t* test, $^{***}p < 0.001$.

Evaluation of the effects of phenothiazine compounds in NOX2 cell-free assay

To prove a direct effect on NOX2, we tested a subset of phenothiazines in a cell-free assay using isolated membranes of the myeloid cell line PLB-985 incubated with recombinant cytosolic factors, FAD and NADPH, and MCLA as a detection probe. The chemiluminescent signal was inhibited by thioridazine (IC_{50} 12.2 ± 1.8 μM), perphenazine (IC_{50} 13.0 ± 1.3 μM), prochlorperazine (IC_{50} 14.6 ± 1.2 μM), and above 50 μM phenothiazine or mesoridazine (Figs. 5a–e). This cell-free assay confirmed that the absence of inhibition by mesoridazine or phenothiazine is not due to a lack of cell permeability, that N-substituted phenothiazines act directly on NOX2, and that the effect observed in cellular assays is not due to cytotoxicity or upstream effectors of NOX2, such as receptor activation or protein kinase C activity.

One of the mechanisms of enzyme inhibition is competition with the substrate of the reaction catalyzed by the enzyme. To address this possibility we performed a competitive NOX2 cell-free assay by measuring reaction velocities as a function of

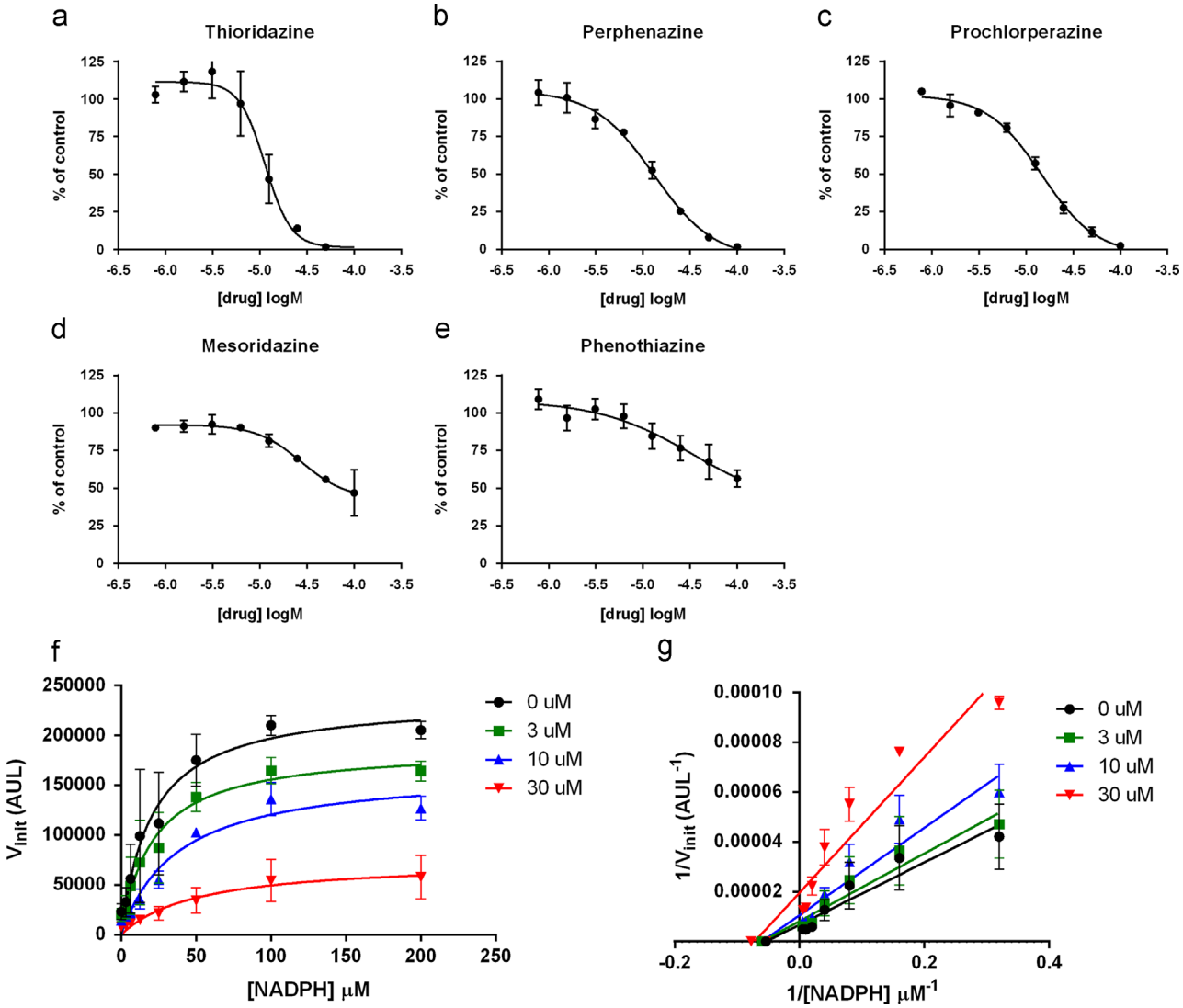

Fig. 5. Characterization of phenothiazine compounds in NOX2 cell-free assays. The activity of selected phenothiazine compounds and their potential mechanism of action were investigated in a NOX2 cell-free assay: membranes from PLB-985 cells were incubated with increasing concentrations of compounds and MCLA luminescence was measured ($n=3$ experiments). (a–e) Concentration–response curves for NOX2 inhibition in a cell-free assay. Thioridazine, perphenazine, and prochlorperazine, but not mesoridazine nor phenothiazine, inhibit NOX2 activity. (f) Michaelis–Menten kinetics of competition assay for NADPH and (g) Lineweaver–Burk fitted representation of the reciprocal data indicates noncompetitive mechanism of action for thioridazine with respect to NADPH in NOX2-containing cell membranes from PLB-985 cells. Velocity of initial reaction (V_{init}) reflects superoxide generation as represented by arbitrary units of luminescence (AUL).

increasing concentrations of NADPH (Fig. 5f). The inhibition modalities were analyzed using nonlinear regression and the reciprocals of the same data points were plotted in a Burke–Lineweaver graph (Fig. 5g). The fact that all best-fitting regression lines intercept the x axis in close vicinity indicate that the K_m values of NADPH are not changed by thioridazine, indicative of a noncompetitive mode of inhibition. The probability of the non-competitive model was confirmed by the extra sum of squares F test (GraphPad Prism 6). Thus the NOX2-inhibitory mechanism of action of thioridazine is noncompetitive for NADPH and remains to be elucidated.

$NADP^+$ electrostatic potential has been extensively studied in aldose reductase by Muzet and co-workers [29]. They showed that $NADP^+$ cofactor displays a large negative potential around the pyrophosphate group and a positive potential around the nicotinamide ring. The electrostatic potential of $NADP^+$ and its spatial orientation suggest the possibility of having a very good electrostatic complementarity with the compounds formed by the ionizable tertiary amine carrying a positive electrostatic potential linked via a propyl to the phenothiazine scaffold having a negative potential (Fig. 3). In this context the nicotinamide would interact with the phenothiazine moiety via π–π stacking.

Enzymatic analysis of such ternary complexes involving cofactors using competition assays reveals generally a noncompetitive behavior as shown, for example, by the aldehyde reductase in ternary complex with coenzyme NADPH and a potent inhibitor [30].

Thus, based on the role played by the electrostatic potential as deduced by the SAR of the molecules, the noncompetitiveness toward NADPH, and the electrostatic potential of $NADP^+$ in NADPH-containing enzymes [29], it can be hypothesized that phenothiazine derivatives interact with NADPH, forming a ternary complex that has been often observed in NADPH-, NADH-, or FAD-containing enzymes [29–31].

In vitro functional assay: redox-dependent myofibroblast differentiation

To demonstrate a functional consequence of NOX inhibition by thioridazine we used the well-described experimental paradigm that NOX-dependent ROS generation, and in particular NOX4 activity, controls fibroblast differentiation to myofibroblast, a key common pathway involved in fibrotic disease and scar formation [32–34]. A human foreskin fibroblast cell line was treated with recombinant TGF-β1, 2 ng/ml, in the presence of the flavoprotein inhibitor DPI, thioridazine, and the NOX-inactive phenothiazine. After 24 h NOX4 and α-SMA expression was evaluated by qPCR. Both NOX4 and α-SMA transcripts were significantly upregulated

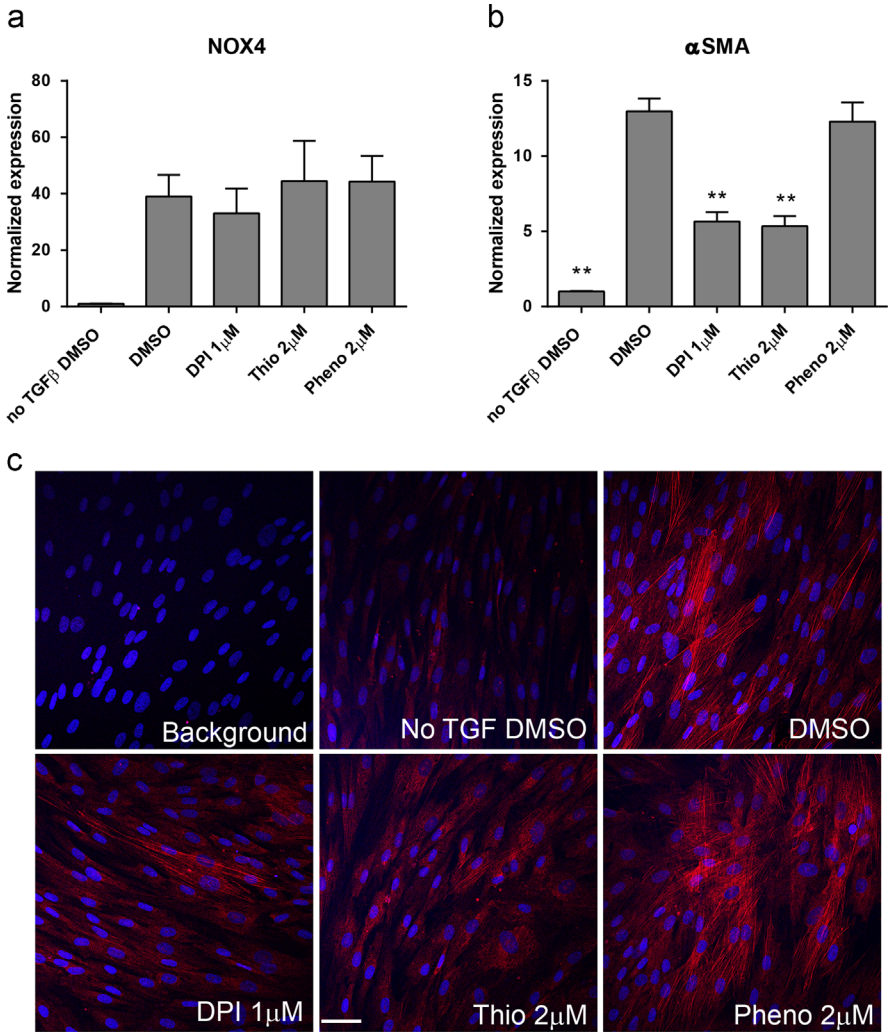

Fig. 6. Thioridazine but not phenothiazine decreases TGF-β1-induced myofibroblast formation by human foreskin fibroblasts (HFFs). (a) NOX4 and (b) α-SMA mRNA expression is induced in HFFs upon TGF-β1 treatment (2 ng/ml, 24 h). Thioridazine but not phenothiazine diminishes α-SMA mRNA expression. Data are presented as fold change of control (no TGF-β1 treatment). (c) Immunostaining with α-SMA antibody shows induction of α-SMA-positive fibers, which is diminished by DPI and thioridazine but not phenothiazine. Nuclei were visualized with DAPI staining. Scale bar, 50 μm. Background, primary antibody was omitted from the staining procedure.

after TGF-β1 treatment (Figs. 6a and b). As expected, DPI (1 μM) prevented TGF-β-induced α-SMA upregulation. Importantly, a low concentration (2 μM) of thioridazine also mitigated the increase in α-SMA to a similar level compared to DPI, a potent inhibitor of NOX. NOX4 expression levels were not affected by any of the inhibitors (Fig. 6a). Visualization of α-SMA protein by immunofluorescent staining showed a similar trend (Fig. 6c). Although it is possible that the action of thioridazine is not mediated only through NOX, the fact that the parent compound phenothiazine was inactive in this differentiation assay argues for this mechanism. Our finding that thioridazine inhibits myofibroblast differentiation confirms that diseases with an exaggerated fibrotic response can be mitigated by small-molecule NOX inhibitors [35]. However, thioridazine and other N-substituted phenothiazines are obviously not optimal NOX inhibitors because they target numerous pathways: their neuroleptic activity is mostly due to the blockade of D2 dopaminergic receptors, and numerous nonpsychiatric effects have been described, including antimicrobial, antihistaminic, and antiemetic, among others [16]. Our results consolidate an additional mechanism of action for these compounds, namely mitigation of NOX-associated oxidative stress.

As of today, only a few studies have characterized NOX inhibitors using a combination of ROS measurements and oxygen consumption [37,13,36], and studies actively searching for artifacts of NOX-derived ROS measurements are few [14]. This study allowed us to identify key substitutions on the phenothiazine moiety that confer NOX inhibition and to formally distinguish NOX inhibitors from nonspecific compounds, such as unsubstituted phenothiazines, which interfere with peroxidase-dependent H_2O_2 detection. Identified molecules now represent validated tools for proof-of-concept experiments and may become a scaffold for further investigation of SARs of phenothiazine-derived molecules and design of new NOX inhibitors devoid of antipsychotic activities. With the increased interest in identifying NOX-targeting therapeutics, the information gained from this family of molecules may prove essential.

Acknowledgments

We thank Sandra Pierredon, Vincent Compan, and Jean-Claude Martinou for advice on Seahorse measurements; Christelle Barraclough and Didier Cholet for assistance with qPCR; Marie-Luce Bochaton-Piallat for providing smooth muscle cells for validation of α-SMA antibody; and Becky Diebold for providing recombinant proteins for membrane assay. This work was supported by a grant from the Swiss innovation promotion agency CTI (KTI-9958.1 PFLS-LS) and by the European Community's Framework program under Grant Agreement Neurinox (Health-F2-2011-278611). Although V.J., L.F.-C., and K.-H.K. are founding members of Genkyotex SA, a company developing NOX inhibitors, there is no conflict of interest as this study describes compounds unrelated to the company.

Appendix A. Supporting information

Supplementary data associated with this article can be found in the online version at http://dx.doi.org/10.1016/j.freeradbiomed.2015.05.023.

References

[1] Leto, T. L.; Morand, S.; Hurt, D.; Ueyama, T. Targeting and regulation of reactive oxygen species generation by Nox family NADPH oxidases. *Antioxid. Redox Signaling* **11**:2607–2619; 2009.

[2] Bedard, K.; Krause, K. H. The NOX family of ROS-generating NADPH oxidases: physiology and pathophysiology. *Physiol. Rev.* **87**:245–313; 2007.

[3] Sorce, S.; Krause, K. H. NOX enzymes in the central nervous system: from signaling to disease. *Antioxid. Redox Signaling* **11**:2481–2504; 2009.

[4] Hecker, L.; Logsdon, N. J.; Kurundkar, D.; Kurundkar, A.; Bernard, K.; Hock, T.; Meldrum, E.; Sanders, Y. Y.; Thannickal, V. J. Reversal of persistent fibrosis in aging by targeting Nox4–Nrf2 redox imbalance. *Sci. Transl. Med. 6*; 2014. 231ra247.

[5] Braunersreuther, V.; Montecucco, F.; Asrih, M.; Pelli, G.; Galan, K.; Frias, M.; Burger, F.; Quindere, A. L.; Montessuit, C.; Krause, K. H.; Mach, F.; Jaquet, V. Role of NADPH oxidase isoforms NOX1, NOX2 and NOX4 in myocardial ischemia/reperfusion injury. *J. Mol. Cell. Cardiol.* **64**:99–107; 2013.

[6] Gorin, Y.; Block, K. Nox as a target for diabetic complications. *Clin. Sci. (London)* **125**:361–382; 2013.

[7] Lambeth, J. D.; Krause, K. H.; Clark, R. A. NOX enzymes as novel targets for drug development. *Semin. Immunopathol.* **30**:339–363; 2008.

[8] Esworthy, R. S.; Kim, B. W.; Chow, J.; Shen, B.; Doroshow, J. H.; Chu, F. F. Nox1 causes ileocolitis in mice deficient in glutathione peroxidase-1 and -2. *Free Radic. Biol. Med.* **68**:315–325; 2014.

[9] Altenhofer, S.; Radermacher, K. A.; Kleikers, P. W.; Wingler, K.; Schmidt, H. H. Evolution of NADPH oxidase inhibitors: selectivity and mechanisms for target engagement. *Antioxid. Redox Signaling* ; 2014. in press.

[10] Jaquet, V.; Scapozza, L.; Clark, R. A.; Krause, K. H.; Lambeth, J. D. Small-molecule NOX inhibitors: ROS-generating NADPH oxidases as therapeutic targets. *Antioxid. Redox Signaling* **11**:2535–2552; 2009.

[11] Maghzal, G. J.; Krause, K. H.; Stocker, R.; Jaquet, V. Detection of reactive oxygen species derived from the family of NOX NADPH oxidases. *Free Radic. Biol. Med.* **53**:1903–1918; 2012.

[12] Heumuller, S.; Wind, S.; Barbosa-Sicard, E.; Schmidt, H. H.; Busse, R.; Schroder, K.; Brandes, R. P. Apocynin is not an inhibitor of vascular NADPH oxidases but an antioxidant. *Hypertension* **51**:211–217; 2008.

[13] Zielonka, J.; Cheng, G.; Zielonka, M.; Ganesh, T.; Sun, A.; Joseph, J.; Michalski, R.; O'Brien, W. J.; Lambeth, J. D.; Kalyanaraman, B. High-throughput assays for superoxide and hydrogen peroxide: design of a screening workflow to identify inhibitors of NADPH oxidases. *J. Biol. Chem.* **289**:16176–16189; 2014.

[14] Zielonka, J.; Lambeth, J. D.; Kalyanaraman, B. On the use of L-012, a luminol-based chemiluminescent probe, for detecting superoxide and identifying inhibitors of NADPH oxidase: a reevaluation. *Free Radic. Biol. Med.* **65**:1310-–1314; 2013.

[15] Feinberg, A. P.; Snyder, S. H. Phenothiazine drugs: structure–activity relationships explained by a conformation that mimics dopamine. *Proc. Natl. Acad. Sci. USA* **72**:1899–1903; 1975.

[16] Sudeshna, G.; Parimal, K. Multiple non-psychiatric effects of phenothiazines: a review. *Eur. J. Pharmacol.* **648**:6–14; 2010.

[17] Cohen, H. J.; Chovaniec, M. E.; Ellis, S. E. Chlorpromazine inhibition of granulocyte superoxide production. *Blood* **56**:23–29; 1980.

[18] Serrander, L.; Cartier, L.; Bedard, K.; Banfi, B.; Lardy, B.; Plastre, O.; Sienkiewicz, A.; Forro, L.; Schlegel, W.; Krause, K. H. NOX4 activity is determined by mRNA levels and reveals a unique pattern of ROS generation. *Biochem. J.* **406**:105-–114; 2007.

[19] Gianni, D.; Taulet, N.; Zhang, H.; DerMardirossian, C.; Kister, J.; Martinez, L.; Roush, W. R.; Brown, S. J.; Bokoch, G. M.; Rosen, H. A novel and specific NADPH oxidase-1 (Nox1) small-molecule inhibitor blocks the formation of functional invadopodia in human colon cancer cells. *ACS Chem. Biol.* **5**:981–993; 2010.

[20] Hadjimitova, V.; Bakalova, R.; Traykov, T.; Ohba, H.; Ribarov, S. Effect of phenothiazines on protein kinase C- and calcium-dependent activation of peritoneal macrophages. *Cell Biol. Toxicol.* **19**:3–12; 2003.

[21] Hadjimitova, V.; Traykov, T.; Mileva, M.; Ribarov, S. Effect of some psychotropic drugs on luminol-dependent chemiluminescence induced by O_2^-, ∗OH, HOCl. *Z. Naturforsch. C* **57**:1066–1071; 2002.

[22] Tan, A. S.; Berridge, M. V. Superoxide produced by activated neutrophils efficiently reduces the tetrazolium salt, WST-1 to produce a soluble formazan: a simple colorimetric assay for measuring respiratory burst activation and for screening anti-inflammatory agents. *J. Immunol. Methods* **238**:59–68; 2000.

[23] Pospisil, P.; Ballmer, P.; Scapozza, L.; Folkers, G. Tautomerism in computer-aided drug design. *J. Recept. Signal Transduction Res* **23**:361–371; 2003.

[24] Hunter, C. A.; Singh, J.; Thornton, J. M. Pi–pi interactions: the geometry and energetics of phenylalanine–phenylalanine interactions in proteins. *J. Mol. Biol.* **218**:837–846; 1991.

[25] Cozzi, F.; Annunziata, R.; Benaglia, M.; Baldridge, K. K.; Aguirre, G.; Estrada, J.; Sritana-Anant, Y.; Siegel, J. S. Through-space interactions between parallel-offset arenes at the van der Waals distance: 1,8-diarylbiphenylene syntheses, structure and QM computations. *Phys. Chem. Chem. Phys.* **10**:2686–2694; 2008.

[26] Hunter, C. A.; Sanders, J. K. M. The nature of.pi.-.pi. interactions. *J. Am. Chem. Soc.* **112**:5525–5534; 1990.

[27] Lee, E. C.; Hong, B. H.; Lee, J. Y.; Kim, J. C.; Kim, D.; Kim, Y.; Tarakeshwar, P.; Kim, K. S. Substituent effects on the edge-to-face aromatic interactions. *J. Am. Chem. Soc.* **127**:4530–4537; 2005.

[28] Arnstein, S. A.; Sherrill, C. D. Substituent effects in parallel-displaced pi–pi interactions. *Phys. Chem. Chem. Phys.* **10**:2646–2655; 2008.

[29] Muzet, N.; Guillot, B.; Jelsch, C.; Howard, E.; Lecomte, C. Electrostatic complementarity in an aldose reductase complex from ultra-high-resolution crystallography and first-principles calculations. *Proc. Natl. Acad. Sci. USA* **100**:8742–8747; 2003.

[30] Carbone, V.; Chung, R.; Endo, S.; Hara, A.; El-Kabbani, O. Structure of aldehyde reductase in ternary complex with coenzyme and the potent 20α-

hydroxysteroid dehydrogenase inhibitor 3,5-dichlorosalicylic acid: implications for inhibitor binding and selectivity. *Arch. Biochem. Biophys.* **479**:82–87; 2008.
[31] Perozzo, R.; Kuo, M.; Sidhu, A.; Valiyaveettil, J. T.; Bittman, R.; Jacobs Jr. W. R.; Fidock, D. A.; Sacchettini, J. C. Structural elucidation of the specificity of the antibacterial agent triclosan for malarial enoyl acyl carrier protein reductase. *J. Biol. Chem.* **277**:13106–13114; 2002.
[32] Cucoranu, I.; Clempus, R.; Dikalova, A.; Phelan, P. J.; Ariyan, S.; Dikalov, S.; Sorescu, D. NAD(P)H oxidase 4 mediates transforming growth factor-beta1-induced differentiation of cardiac fibroblasts into myofibroblasts. *Circ. Res.* **97**:900–907; 2005.
[33] Hecker, L.; Vittal, R.; Jones, T.; Jagirdar, R.; Luckhardt, T. R.; Horowitz, J. C.; Pennathur, S.; Martinez, F. J.; Thannickal, V. J. NADPH oxidase-4 mediates myofibroblast activation and fibrogenic responses to lung injury. *Nat. Med* **15**:1077–1081; 2009.
[34] Sampson, N.; Koziel, R.; Zenzmaier, C.; Bubendorf, L.; Plas, E.; Jansen-Durr, P.; Berger, P. ROS signaling by NOX4 drives fibroblast-to-myofibroblast differentiation in the diseased prostatic stroma. *Mol. Endocrinol.* **25**:503–515; 2011.
[35] Jiang, F.; Liu, G. S.; Dusting, G. J.; Chan, E. C. NADPH oxidase-dependent redox signaling in TGF-beta-mediated fibrotic responses. *Redox Biol* **2**:267–272; 2014.
[36] Hancock, J. T.; Jones, O. T. The inhibition by diphenyleneiodonium and its analogues of superoxide generation by macrophages. *Biochem. J.* **242**:103–107; 1987.
[37] Jaquet, V.; Marcoux, J.; Forest, E.; Leidal, K. G.; McCormick, S.; Westermaier, Y.; Perozzo, R.; Plastre, O.; Fioraso-Cartier, L.; Diebold, B.; Scapozza, L.; Nauseef, W. M.; Fieschi, F.; Krause, K. H.; Bedard, K. NADPH oxidase (NOX) isoforms are inhibited by celastrol with a dual mode of action. *Br. J. Pharmacol.* **164**:507–520; 2011.
[38] Serrander, L.; Jaquet, V.; Bedard, K.; Plastre, O.; Hartley, O.; Arnaudeau, S.; Demaurex, N.; Schlegel, W.; Krause, K. H. NOX5 is expressed at the plasma membrane and generates superoxide in response to protein kinase C activation. *Biochimie* **89**:1159–1167; 2007.
[39] Tucker, K. A.; Lilly, M. B.; Heck Jr. L.; Rado, T. A. Characterization of a new human diploid myeloid leukemia cell line (PLB-985) with granulocytic and monocytic differentiating capacity. *Blood* **70**:372–378; 1987.
[40] Banfi, B.; Clark, R. A.; Steger, K.; Krause, K. H. Two novel proteins activate superoxide generation by the NADPH oxidase NOX1. *J. Biol. Chem.* **278**:3510–3513; 2003.
[41] Suter, D. M.; Cartier, L.; Bettiol, E.; Tirefort, D.; Jaconi, M. E.; Dubois-Dauphin, M.; Krause, K. H. Rapid generation of stable transgenic embryonic stem cell lines using modular lentivectors. *Stem Cells* **24**:615–623; 2006.
[42] Rinaldi, M.; Moroni, P.; Paape, M. J.; Bannerman, D. D. Evaluation of assays for the measurement of bovine neutrophil reactive oxygen species. *Vet. Immunol. Immunopathol.* **115**:107–125; 2007.
[43] Diebold, B. A.; Bokoch, G. M. Molecular basis for Rac2 regulation of phagocyte NADPH oxidase. *Nat. Immunol.* **2**:211–215; 2001.
[44] Bromberg, Y.; Pick, E. Activation of NADPH-dependent superoxide production in a cell-free system by sodium dodecyl sulfate. *J. Biol. Chem.* **260**:13539–13545; 1985.
[45] Nauseef, W. M. Isolation of human neutrophils from venous blood. *Methods Mol. Biol.* **412**:15–20; 2007.
[46] Vandesompele, J.; De Preter, K.; Pattyn, F.; Poppe, B.; Van Roy, N.; De Paepe, A.; Speleman, F. Accurate normalization of real-time quantitative RT-PCR data by geometric averaging of multiple internal control genes. *Genome Biol.* 3; 2002. RESEARCH0034.